# Growth of two-dimensional WS2 thin films by reactive sputtering

Michelle Villamayor, Andreas Lindblad, Fredrik Johansson, Tuan Tran, Ngan Pham, Daniel Primetzhofer, Nomi L.A.N. Sorgenfrei, Erika Giangrisotomi, Alexander Föhlisch, Pedro Lourenço, et al.

Vacuum 188 (2021) 110205

Contents lists available at ScienceDirect

Vacuum

journal homepage: http://www.elsevier.com/locate/vacuum

# Growth of two-dimensional $WS_2$ thin films by reactive sputtering

Michelle Marie S. Villamayor [a], Andreas Lindblad [b], Fredrik O.L. Johansson [b], Tuan Tran [c], Ngan Hoang Pham [a], Daniel Primetzhofer [c], Nomi L.A.N. Sorgenfrei [d,e], Erika Giangrisotomi [e], Alexander Föhlisch [d,e], Pedro Lourenço [f], Romain Bernard [f], Nadine Witkowski [f], Geoffroy Prévot [f], Tomas Nyberg [a,*]

[a] Division of Solid State Electronics, Department of Electrical Engineering, Angstrom Laboratory, Uppsala University, Box 65, SE-751 03, Uppsala, Sweden
[b] Division of X-ray Photon Science, Department of Physics and Astronomy, Uppsala University, Box 516, SE-751 20, Uppsala, Sweden
[c] Division of Applied Nuclear Physics, Department of Physics and Astronomy, Uppsala University, Box 516, SE-751 20, Uppsala, Sweden
[d] Institut für Physik und Astronomie, Universität Potsdam, Karl-Liebknecht-Straße 24/25, 14476, Potsdam, Germany
[e] Institute for Methods and Instrumentation for Synchrotron Radiation Research, Helmholtz-Zentrum Berlin für Materialien und Energie GmbH, Albert-Einstein-Straße 15, 12489, Berlin, Germany
[f] Sorbonne Université, CNRS, Institut des NanoSciences de Paris, INSP, F-75005, Paris, France

ARTICLE INFO

*Keywords:*
Reactive sputtering
Two-dimensional
Thin film
Tungsten sulfide
Transition metal dichalcogenide

ABSTRACT

We have deposited $WS_2$ thin films on Si, $SiO_2$/Si, and sapphire substrates by reactive sputtering from a $WS_2$ target in an Ar/$H_2S$ atmosphere. We demonstrate that it is possible to deposit (001)-textured tungsten sulfide films that are thicker than 100 nm. However, the sputtered films are slightly substoichiometric with a composition of $WS_{1.94}$. Films were deposited at different processing pressures (0.67 Pa–6.67 Pa), substrate temperatures (up to 700 °C) and relative amounts of $H_2S$ (0%–100%) in the gas mixture. Structure, morphology, composition, and resistivity of the films were investigated for the different processing conditions. Results from X-ray diffraction show that best crystallization was achieved for the highest substrate temperatures and processing pressures. We show that the addition of $H_2S$ may help obtaining fully stoichiometric films and reduce the risk of losing the (001) texture for thicker films. The challenges of obtaining an epitaxial and fully stoichiometric film are pointed out and suggestions on how to modify the process parameters in order to obtain films with even higher quality are presented.

## 1. Introduction

The discovery of graphene triggered extensive research efforts focused on synthesis and characterization of promising two-dimensional (2D) materials [1–4]. An issue with graphene is its lack of a band-gap, making it difficult to integrate this material into electronic applications. Therefore, the focus has lately shifted to semiconducting 2D materials. More than 5000 different compounds featuring a layered 2D structure have been identified so far [5]. A large number of 2D materials have already been successfully synthesised and thoroughly studied. Examples of such developed 2D materials are graphene, hexagonal boron nitride (h-BN), transition metal dichalcogenides (TMDCs), MXenes, silicene [6], phosphorene, germanene, etc. [2,7]. These compounds hold large diversity of electronic properties, ranging from insulators and semiconductors over to semimetals and metals.

TMDCs are a family of semiconducting 2D materials that has attracted much interest recently. Unlike graphene which has all the atoms in the same plane, each monolayer (ML) of a TMDC material normally consists of one plane of transition-metal atoms sandwiched between two planes of chalcogen atoms with a covalent bonding arranged in a trigonal prismatic network. The monolayers are bonded to each other by weak van der Waals forces that can easily be broken. There are no dangling bonds on either surface of each layer making the surfaces very stable and non-reactive. Among the transition metals, the most studied are Mo or W, while the chalcogen are S, Se, or Te. These materials with S or Se typically have optical band gaps in the range of 1–2 eV combined with a substantial exciton binding energy resulting in even larger electronic band gaps [7,8]. $WTe_2$ is on the other hand a semimetal. Moreover, the TMDCs typically have tuneable bandgaps that decrease with the film thicknesses and there is also a transition from

* Corresponding author.
*E-mail address:* tomas.nyberg@angstrom.uu.se (T. Nyberg).

https://doi.org/10.1016/j.vacuum.2021.110205
Received 27 January 2021; Received in revised form 12 March 2021; Accepted 13 March 2021
Available online 17 March 2021

direct to indirect band gap as the film thickness goes from one monolayer to several monolayers. In addition, these materials generally have a rather high carrier mobility (>100 $cm^2\ V^{-1}\ s^{-1}$) [7,8]. The most frequently studied TMDC materials are $MoS_2$ followed by $WS_2$.

This work deals with $WS_2$ which has superior electronic properties compared to several other TMDCs as described below. Further, $WS_2$ exhibits a very strong light-matter interaction and it has been shown that a ML of $WS_2$ can absorb up to 10% of the incident visible light [9,10]. This property implies a very large absorption coefficient of $\approx 1.5 \times 10^6$ $cm^{-1}$ [9]. $WS_2$ has therefore potential in various optoelectronic devices, e.g. photodetectors [11] and light-emitting devices [12]. It has further been demonstrated that $WS_2$ can be integrated in high-performance memristor devices [13]. Moreover, $WS_2$ has the highest theoretically calculated electron and hole mobilities of all $MX_2$ (M = Mo, W; X = S, Se) materials.

The distance between each layer in 2D $WS_2$ is about 0.65 nm. There are no dangling bonds on either surface of each layer making the surfaces very stable and nonreactive. Due to the weak van der Waal forces between the layers, the $WS_2$ crystal can be easily exfoliated. The stable coordination of W is trigonal prismatic, referred to as the 2H phase (which is the polytype found in nature). The unit cell of 2H $WS_2$ extends over two layers with the S atoms of the second layer sitting on top of the W atoms of the first layer and vice versa [7,8]. The optical gap changes from a direct gap of 2 eV for ML $WS_2$, to an indirect gap of around 1.5 eV for 2 ML and approximately 1.3 eV (indirect gap) for 5 ML and thicker films. Thus, bulk properties are obtained for 5 ML thick films. This property is analogous to other TMDC materials. It should be kept in mind that there is a difference between the electronic band gap and the optical gap. This difference is determined by the exciton binding energy which is 0.7 eV for ML thick $WS_2$ and significantly smaller for thicker $WS_2$ films [7,8]. Thus the electronic band gap is approximately 2.7 eV for one ML thick $WS_2$ films. When considering all phonon branches, the room temperature (RT) electron and hole mobilities in ML $WS_2$ are found to be 320 and 540 $cm^2\ V^{-1}s^{-1}$, respectively [14]. When only long wave acoustic phonons are considered, ML $WS_2$ is predicted to have an RT electron mobility of 1103 $cm^2\ V^{-1}s^{-1}$ [15]. This fact indicates that $WS_2$ has an enormous potential as transistor channel material. The thinness will suppress short-channel effects, which enables further downscaling of transistors. Transistors made from 2D $WS_2$ have demonstrated large ON/OFF current ratios (>$10^5$) [16,17]. However, the carrier mobilities of such $WS_2$-based transistors are still relatively low as compared with theoretical predictions. High-performance transistors will require a high quality $WS_2$ as channel material. Crystal defects, such as S vacancies, are an intrinsic reason for significantly reduced carrier mobility [18,19]. Structural defects must therefore be avoided or repaired in order to realize high mobility 2D $WS_2$ transistors.

Apart from the ability to synthesize high quality $WS_2$ films, the technique used for such synthesis must also be scalable and cost effective in order to enable integration into various electronic applications. The weak van der Waals interaction between the layers in the $WS_2$ crystal facilitates top-down synthesis techniques such as mechanical exfoliation by scotch tape. Other top-down techniques include liquid phase exfoliation and various types of intercalation followed by exfoliation [8] Such top-down methods are, however, not scalable and viable for large scale production and further they are not suitable for electronic applications due to the presence of process residues. There are solution-based bottom-up routes which involve chemical reactions in the liquid phase at elevated temperatures that are suitable for high-yield mass production but these methods do not allow for very high controllability over the crystal quality and electrical properties [8]. Another method is post-sulfurization/annealing (>650 °C) of seed films consisting of $W/WO_x$ [20–23]. However, the quality of the 2D $WS_2$ film depends strongly on the quality of the seed film and sulfurization process. Normally, the uniformity and quality of the films is relatively poor with small grain sizes and high defect density. One example of a scalable technique that also enables high quality films in industrial production is chemical vapor deposition (CVD) [7]. Kang et al. demonstrated CVD synthesis of one ML thin $WS_2$ films over a full 4" wafer for the first time [24]. However, this $WS_2$ material exhibits an electron mobility of 5 $cm^2\ V^{-1}s^{-1}$ and has a very low growth rate of 26 h for full coverage over a wafer. Furthermore, the grain size is relatively small (about 1 μm) with random in-plane orientation. Other groups have also demonstrated growth of $WS_2$ thin films by CVD [25–27]. Another example of a scalable, cheap, relatively simple, and industrially compatible technique is sputtering. To be able to deposit a $WS_2$ film without the need for post-sulfurization, it is necessary to provide sulfur as a source material in the process. Sulfur can be provided from the target ($WS_2$ target), from a reactive gas ($H_2S$), from an additional sulfur evaporation source, or from a combination of these. Extensive and thorough work has been carried out by Ellmer et al. [28–34], where $WS_2$ films have been sputtered from W-target in Ar/$H_2S$ gas mixtures, as well as Levy et al. [35–37], who used a $WS_2$-target in Ar/$H_2S$ gas mixtures. There are some general challenges and issues with sputtering of 2D TMDC (including $WS_2$) films. The sputtered films are often substoichiometric because of the very high vapor pressure of the chalcogen (i.e. sulfur) which results in preferential desorption of the chalcogen (S) from the surface of the growing film before forming a chemical bond with a metal atom (W). Other mechanisms responsible for substoichiometric films include preferential re-sputtering of sulfur from the $WS_2$ film as well as the different deposition rate profiles for S and W throughout the chamber [38]. These mechanisms lead to sulfur vacancies/lattice defects that are responsible for transformation of the film growth from the preferred structure in which the layers are parallel to the substrate, i.e. (001)-texture, to an undesirable structure where the layers are perpendicular to the substrate, i.e. (100)/(101)-texture. Moreover, the vacancies create energy levels close to the conduction band resulting in an increased carrier density and a lower carrier mobility [39,40]. Another issue is the small crystalline domain sizes due to high nucleation density resulting in an increased amount of grain boundaries and defects/misalignments. These issues degrade the electronic performance, especially the carrier mobility, of the material despite a fairly good structural quality [3,4,28].

In this work, we deposit $WS_2$ thin films by reactive pulsed direct current (DC) sputtering from a $WS_2$ target in Ar/$H_2S$ gas mixture. The choice of having sulfur in the target as well as in the reactive gas is based on the fact that sputtering normally gives sulfur deficient films. Ellmer et al. concluded that additional sulfur in the sputtering atmosphere may help to eliminate sulfur vacancies and thereby reduce the probability of transforming the film growth from (001)-texture to (100)/(101)-texture [29].

We investigate the influence of the processing pressure, substrate temperature, and gas mixture on the composition, structure and crystalline quality of the films. The films are characterized by X-ray diffraction (XRD), transmission electron microscopy (TEM), Rutherford backscattering spectrometry (RBS) and nuclear reaction analysis (NRA). The purpose of the work is to expand the processing parameter space with respect to previous work to be able to increase the level of understanding regarding the $WS_2$ film growth during sputtering and above all to be able to modify the process parameters to obtain stoichiometric high quality 2D $WS_2$ films. The effects of the substrate temperature, the processing pressure, and the gas mixture during growth are studied. In the following, we demonstrate the growth of nearly stochiometric $WS_2$ films with thicknesses surpassing 100 nm. These films also display a good crystalline quality and layered structure.

## 2. Experimental details

The $WS_2$ thin films were reactively sputtered from a 4 inch $WS_2$ (99.8% purity) target using pulsed DC with a pulsing frequency of 20 kHz which was supplied by a Huttinger PFG 3000 DC power supply equipped with Advanced Energy Sparc-le 20 pulsing units. $H_2S$ (purity 99.5%) was used as a process gas, either pure or together with Ar. The substrate table (4 inch) was electrically floating and was rotating with

approximately 20 rpm. We used a rebuilt von Ardenne CS600 cluster sputtering system equipped with three magnetrons, all facing the substrate at an angle of 45° and with target-to-substrate distance of 16 cm. The base pressure was in the range of $10^{-5}$ Pa. The heater installed under the substrate could give a maximum substrate temperature of around 700 °C. The substrates used were oxidized Si (>100 nm $SiO_2$), Si, and (0001) sapphire. The target power was kept at 200 W. The film thicknesses were around 20 nm and above.

XRD was carried out at a Phillips X'pert MRD diffractometer using Cu $K_\alpha$ radiation equipped with a parallel plate collimator. The patterns were measured in θ−2θ mode. The powder diffraction file used for reference was the 2H phase tungsten sulfide (PDF 04-003-4478). The four point probe measurements were carried out by a commercial sheet resistance/resistivity measurement system from Advanced Instrument Technlogogy (AIT) Model: CMT-SR2000 N. Ion beam analysis in the form of RBS and NRA was performed using a 5 MV pelletron tandem accelerator at Uppsala University. For RBS a beam of 2 MeV $He^+$ primary ions was employed. For NRA, we utilized the resonant $^1H(^{15}N, \alpha\gamma)^{12}CC$ nuclear reaction, scanning the beam energy. Further details on the experimental set-ups can be found elsewhere [41]. For quantification from RBS-spectra, we employed SIMNRA [42]. Quantification in NRA was done by relative measurements using an H-implanted Si-target as a standard.

## 3. Results and discussion

### 3.1. Influence of the substrate temperature

A series of depositions was carried out for the following substrate temperatures: room temperature (RT), 500 °C, 600 °C, and 700 °C. The total processing pressure was kept at 6.67 Pa in pure Ar having a flow of 20 sccm. Fig. 1a shows the XRD-diffractograms for all films. A perfect 2D film with (001)-texture would only show very sharp peaks at (002), (004), (006) and (008). We use the full width at half maximum (FWHM) of the (002) peak at around $2\theta = 14.4^{\circ}$ as a measure of the film quality. Using the Scherrer equation (with c = 0.885) [43], we obtain that grain sizes vary between 4 nm and 12 nm when the FWHM changes from $2^{\circ}$ to $0.7^{\circ}$ [43]. The diffractogram was fitted in a least squares procedure to Voigt functions, the Lorentzian part was used to extract the FWHM for the Scherrer equation.

Further, it is not desirable to have vertical plane growth which is manifested by peaks at $2\theta = 32.8^{\circ}$ and $2\theta = 34.4^{\circ}$, corresponding to (100) and (101) peaks respectively. If present, the small sharp peaks at around $55^{\circ}$ originate from the substrate holder. We define a texture parameter, $c_{tex}$, as I(002)/I(100), where I signifies the intensity of a certain diffraction peak. It is not surprising to see that the film deposited at RT has no distinguishable XRD peaks and lacks any periodic structure, including a layered 2D structure, and it is therefore not possible to define FWHM or texture parameter for this film. Fig. 1b shows the FWHM of the (002) diffraction peak as well as $c_{tex}$ vs. the substrate temperature. From Fig. 1 it is clearly seen that as temperature increases, the FWHM is significantly reduced from $2.0^{\circ}$ to $0.7^{\circ}$ and the texture parameter is dramatically increased. Consequently, the quality of the sputtered film increases at higher temperatures. The fact that high temperature is beneficial for the synthesis of high-quality $WS_2$ films has been observed by others [7,28,44].

### 3.2. Influence of the processing pressure

To investigate the influence of the processing pressure, a series of depositions was carried out at different processing pressures: 0.67 Pa, 1.33 Pa, 4.00 Pa, 5.33 Pa, and 6.67 Pa. The substrate temperature was kept at 700 °C and the processing gas was pure $H_2S$ (20 sccm). Fig. 2a shows the XRD-diffractograms for all films and Fig. 2b shows the FWHM and the texture parameter vs. processing pressure. The (100)/(101) peaks are clearly visible at pressures below 5.33 Pa and are barely

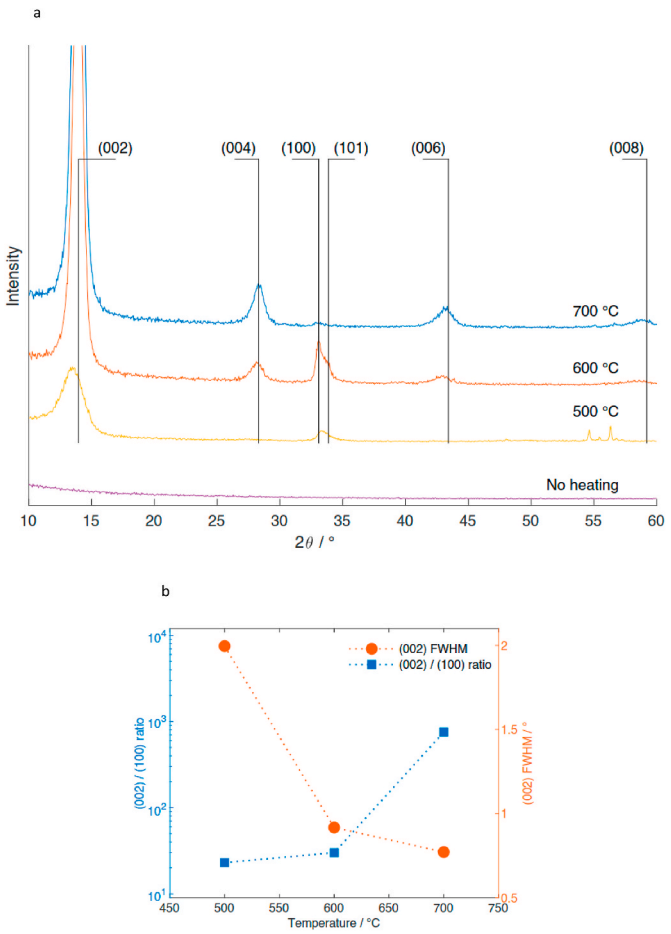


**Fig. 1.** (a) XRD for films deposited at different substrate temperatures in pure Ar at a pressure of 6.67 Pa; (b) FWHM of the (002) peak and the ratio between the intensities of the (002) and (100) peaks vs. substrate temperature. Error bars are within the size of the markers.

detectable at 6.67 Pa. This pressure dependence is also seen in Fig. 2b where the general trend is that the texture parameter is improving with the pressure. The point at 0.67 Pa is an exception to this trend. However, at this high substrate temperature the process features a very high adatom surface diffusion and tends to maintain a good crystallinity, and consequently a low FWHM, that is only weakly dependent on the pressure. In fact, the FWHM is less or equal for all films at high temperature regardless of pressure (in Fig. 2b) as compared to the high temperature film in Fig. 1b. With domain sizes varying from 13 to 30 nm computed from the Scherrer equation. This is on the same order as the film thicknesses.

This means that crystal defects or sulfur vacancies that may occur during growth as a result from energetic bombardment will effectively be annealed owing to the high temperature. One should keep in mind that $WS_x$ may crystallize in a 2D layered structure even for $x \leq 1.7$ [31]. Therefore, the high temperature may give a high quality layered 2D structure although the material is significantly substoichiometric. RBS measurements (not shown) confirm that the films deposited at 0.67–1.33 Pa have a [S]/[W] ratio of about 1.8 while the same ratio is higher at higher pressures. A low [S]/[W] ratio is undesirable since sulfur vacancies results in a lower carrier mobilities [39,40]. Also, such sulfur vacancies are nucleation seeds for $WS_2$ crystallites growing in the (100)/(101) orientation, making it more likely that the film growth switches over to the undesired (100)/(101) growth. The compositional trend versus processing pressure can be explained by the preferential re-sputtering of sulfur from the growing film due to energetic particle bombardment, which is facilitated by a long mean free path as a

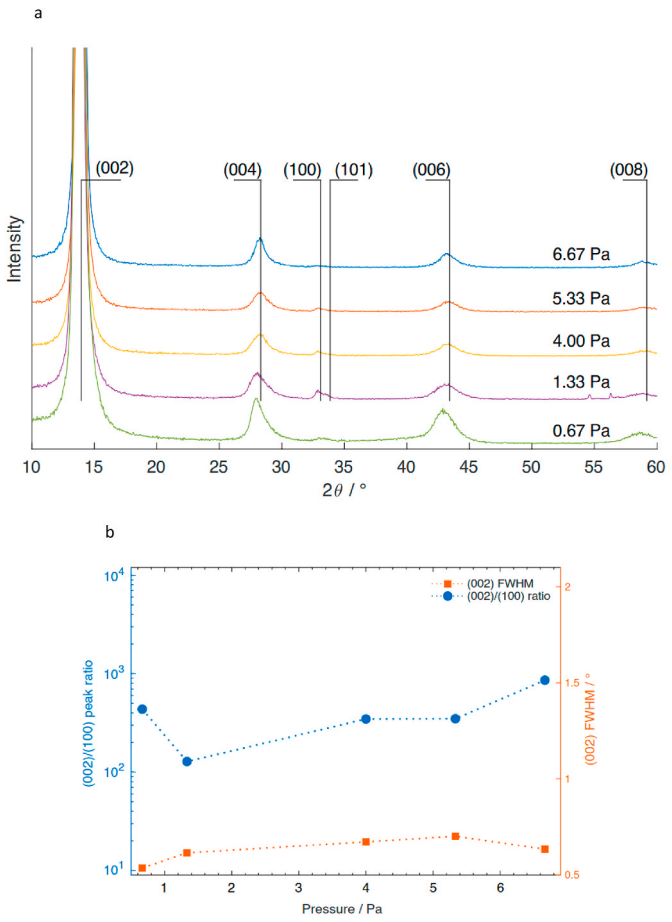


**Fig. 2.** (a) XRD for films deposited at different processing pressures in pure $H_2S$ at a substrate temperature of 700 °C; (b) FWHM of the (002) peak and the ratio between the intensities of the (002) and (100) peaks vs. pressure. Error bars are within the size of the markers.

consequence of a low processing pressure [29,31]. To eliminate this effect, the pressure should be high enough to thermalize all energetic particles from the target [45]. A processing pressure of 6.67 Pa is sufficient to achieve this.

### 3.3. Influence of the gas mixture

From the depositions at different temperatures and pressures it is concluded that the overall best film quality is obtained at high processing pressure and high substrate temperature. This is in line with earlier studies [3,7,29,35,44]. However, to our knowledge, there is no study on films sputtered from a $WS_2$ target at these high pressures/temperatures where the processing gas is varied from 0 to 100% $H_2S$. To investigate the influence from the processing gas composition, a series of depositions was carried out with 0%, 20%, 40%, 60%, 80%, and 100% of $H_2S$ in the $H_2S$/Ar gas mixtures. The processing pressure was 6.67 Pa and the substrate temperature was kept at 700 °C. Fig. 3a shows the XRD for all films, Fig. 3b shows the FWHM and the texture parameter vs. $H_2S$ content, and Fig. 3c shows the [S]/[W] ratio as measured from RBS and the hydrogen content as measured by NRA. From the XRD, specifically the texture parameter and FWHM, it seems as if the crystalline quality is best at around 60–80% $H_2S$. Also the [S]/[W] ratio is the highest (1.94) at 60% $H_2S$ (and 0% $H_2S$). This ratio falls to 1.9 for 80% $H_2S$ and to 1.86 for 100% $H_2S$. It is not obvious why the S content in the film decreases when the S content in the chamber increases as a consequence of higher supply of $H_2S$ (crystallite domain size 18 nm for the smallest FWHM). Nonetheless, this trend was also observed by

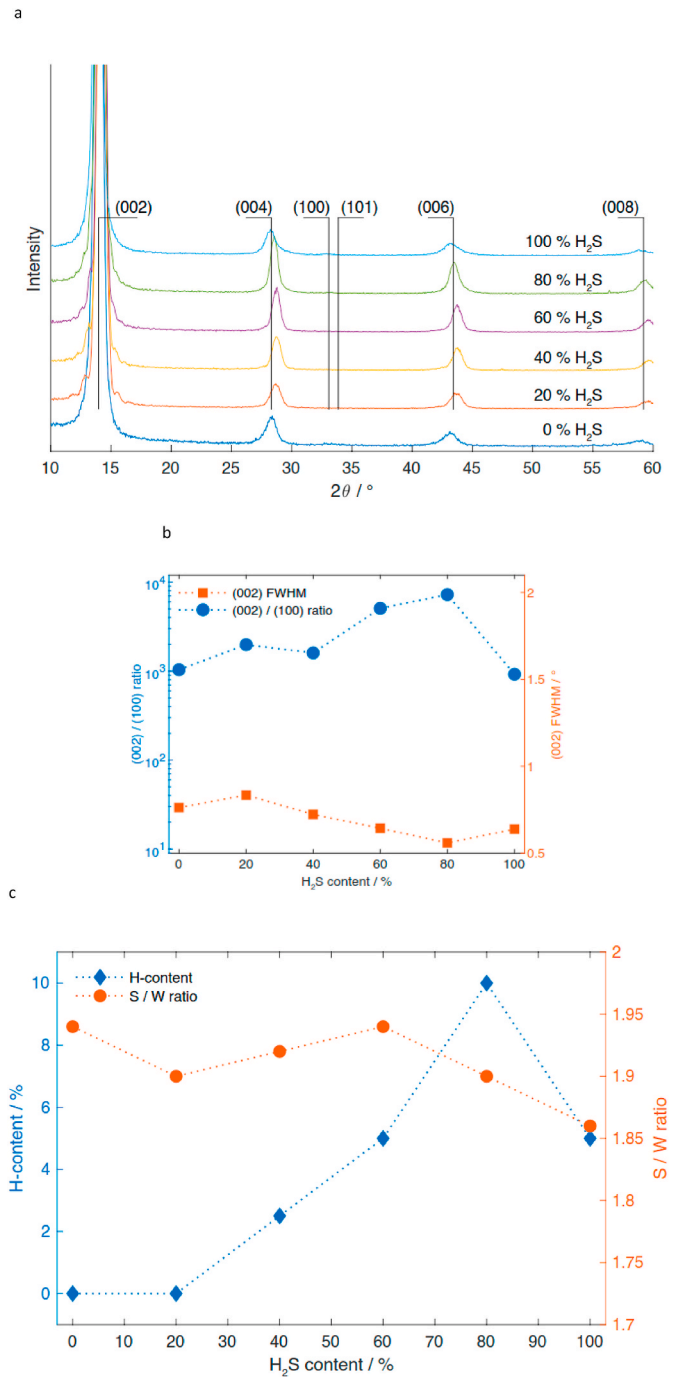


**Fig. 3.** (a) XRD for films deposited with different amounts of $H_2S$ in the $H_2S$/Ar gas at a substrate temperature of 700 °C and a pressure of 6.67 Pa; (b) FWHM of the (002) peak and the ratio between the intensities of the (002) and (100) peaks vs. the relative amount of $H_2S$; (c) the [S]/[W] ratio as measured from RBS and the hydrogen content measured by NRA vs. the relative amount of $H_2S$. Error bars are within the size of the markers.

Ellmer et al. during sputtering from a W target in different $H_2S$/Ar gas mixtures [29]. They argued that since the gas phase contains an oxidizing (S) as well as a reducing component (H), it is not clear whether the required sulfurization really occurs. Further, he particularly referred to the high amount of reactive hydrogen, i.e. atomic hydrogen, which is formed in the plasma leading to a much more pronounced reducing effect compared to a thermal $H_2S$ treatment. Given the rather complex and non-linear processes in a plasma, it may very well happen that the relative strength of the oxidizing component and the reducing

component is varying with the $H_2S$ concentration. A similar mechanism may be responsible for the hydrogen content versus % $H_2S$ as estimated from NRA and presented in Fig. 3c, which shows that the hydrogen content in the film is peaking at around 10% for 80% $H_2S$ whilst not detectable up to 20% $H_2S$ in the processing gas. These hydrogen contents are comparable with those found in other studies [29,32]. It is interesting to note that the significant contents of hydrogen do not seem to have a negative impact on the film quality determined from the XRD and [S]/[W] ratio. However, there seem to be slight shifts for the XRD peaks for 20–80% of $H_2S$ in the gas mixture, possibly related to a change in lattice constant due to hydrogen intercalation between the S–W–S layers. Nonetheless, significant amounts of hydrogen are detrimental for the electronic properties and a method of increasing the [S]/[W] ratio without adding hydrogen to the film would be desirable, e.g. by adding more sulfur vapor. Yang et al. claim to have deposited stoichiometric 2D $WS_2$ thin films by DC magnetron sputtering from metallic targets in a vaporized sulfur ambient using a substrate temperature of 750 °C [44]. This technique can be considered to be a hybrid process between sputtering and evaporation. It is crucial that the sputter deposited metal is uniformly deposited in such process since the added sulfur will only contribute to the film growth where there is tungsten to react with. Mutlu et al. tried to synthesize $WS_2$ film by post-sulfurization of W metal films by S-vapor. However, due to the island-like morphology of the W metal seed layer, the resulting $WS_2$ film is discontinuous with non-uniform thickness [20]. Jung et al. sulfurized differently thick W films by S-vapor and they found that the structural orientation of the obtained $WS_2$ films was strongly related to the sputtered W metal film thickness. The layer orientation of $WS_2$ was vertical to the substrate for thick W seed films (15 nm), while it was parallel to the substrate for very thin W seed films (2 nm). The reason for this is a significant volume expansion for the conversion of W seed to $WS_2$ film due to the insertion of S atoms. When the seed layer is very thin, the horizontal volume expansion can be accommodated. For thicker continuous W films, the horizontal volume expansion cannot be accommodated upon sulfurization. As a result, the sulfurized thicker films have a vertically aligned orientation [22]. Similar results have been observed for sulfurization of 50 nm thick sputtered W films that were sulfurized in gas mixture containing $H_2S$. Here a vertical structure was obtained at sulfurization temperatures below 950 °C while 1000 °C was enough to convert the complete film into a fully stoichiometric $WS_2$ film with horizontally aligned orientation [46]. Altogether, the studies referred above indicate that post-sulfurization to increase the [S]/[W] ratio in the films is possible without adding hydrogen to the film. One should remember that post-sulfurization in $H_2S$ without plasma will not produce any atomic hydrogen that is responsible for the reduction of the films and most likely also the incorporation of hydrogen into the film. The studies also indicate that the post-sulfurization of pure metal films may be difficult and result in non-uniform films with low quality and undesired structure unless the temperature is unrealistically high. However, if the films already have a good structure and well-defined horizontally aligned layers but are slightly sulfur deficient, it is likely that a post-sulfurization in $H_2S$ at elevated temperature, after the plasma is switched off, will increase the [S]/[W] ratio. Indeed, Lignier et al. report that such annealing in an Ar/$H_2S$ atmosphere resulted in an increase in the [S]/[W] ratio [47]. It remains an open question whether additional hydrogen in the film will be reduced during such post-annealing. Nonetheless, an annealing step in $H_2S$ would not only increase the sulfur content but also increase the grain sizes [47]. Apart from sulfur vacancies, small grain sizes also give rise to low carrier mobilities. The Scherrer results points to 80% $H_2S$ together with a higher temperature yielding largest coherent domain sizes.

Fig. 4a and b show TEM images for films deposited at 0% $H_2S$ (i.e. pure Ar) and 60% $H_2S$ respectively. There are no significant differences between the films but careful inspection of the images reveals that the film deposited in pure Ar (Fig. 4a) exhibits a higher defect density, mostly dislocations, visible as bifurcations and shorter lattice planes of S–W–S layers. This observation further corroborates the observation that the film crystallinity is best at around 60–80% $H_2S$ in the gas mixture. Furthermore, a close inspection of Fig. 4a and b reveal a top surface with signs of island growth that has been terminated upon coalescence resulting in defects from layers that have eclipsed each other. However, the growth continues to progress along the original horizontal direction. Although we refer to this as layer-by-layer growth, a more precise description would probably be layer-by-layer growth with some elements of island growth (Stranski-Krastanov growth mode). The locally introduced defects can be readily observed and may serve as nucleation centers for vertical growth but does not necessarily have to do so. There is however no detectable growth of layers perpendicular to the substrate in these film. This is confirmed by the absence of (100)/(101) peaks in the corresponding diffractograms.

### 3.4. Thicker films and different substrates

The [S]/[W] ratio is the result of a complex balance between the addition of W and S. This is particularly true when the S atoms originate from different sources, such as sputtered S-atoms from the target and radicals from $H_2S$ gas produced in the plasma confined close to the target. The plasma also produces hydrogen radicals which may be reducing the S-content in the films as described above. Another potential source of S is the outgassing of sulfur from previous sulfur rich deposits

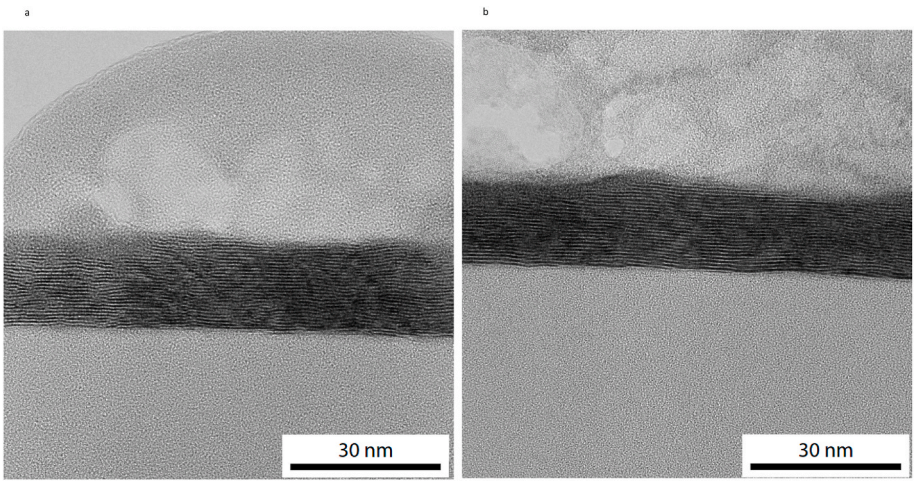


**Fig. 4.** TEM images of films deposited at 700 °C and 6.67 Pa with a $H_2S$/Ar gas mixture of: (a) 0% $H_2S$ (i.e. pure Ar): (b) 60% $H_2S$.

on the chamber walls. This source of sulfur may be more significant if the preceding depositions were carried out at lower temperatures since there exists amorphous $WS_3$ and $WS_5$ phases at temperatures below 250 °C [28,48]. This means that high sulfur content phases may be deposited onto parts of the chamber walls having temperatures lower than this.

Sputtered $WS_2$ and other TMDCs are known to grow in a layer-by-layer fashion with the basal plane parallel to the surface for the first 2–50 layers if sufficient energy to overcome kinetic crystallization barriers is provided. This growth mechanism is a result of the low surface energy of the material. Since a system is most stable when its total energy is minimized, coating a surface with a different material having a lower surface energy, e.g. $WS_2$ on top of $SiO_2$, facilitates a layer-by-layer growth. After a period of horizontal growth, a transition to different growth modes may occur. This transition is triggered by crystal defects such as sulfur vacancies, grain boundaries, misalignment or bifurcation of the basal planes so that the crystal edge is exposed. The edge of the crystal may then act as seed location for growth of planes that are vertically oriented with respect to the substrate surface [3,29]. The surface energy at the edge of the crystal is significantly higher than the basal plane. Consequently, growth occurs much faster at these edges as the driving force for atomic attachment is dramatically higher. In fact, the surface energy of the edge sites is almost 2 orders of magnitude higher than that of the basal plane [22]. At high deposition temperatures, deposited sulfur is diffusing around on top of the rather inert basal plane until it is either reacting with W at the edge of the crystal or desorbed from the surface. The reduced sulfur content in the films with increasing temperature is due to the increased vapor pressure of sulfur that will desorb from the substrate prior to reaction with W. A high sulfur content in the film is promoted by a high S-content in the gas phase together with a low film growth rate, which will allow all the W to react with S. Minimizing sulfur vacancies is a prerequisite for a continuous layer-by-layer growth. Regula et al. and Ellmer et al. have indicated a few tens of nm of (001)-textured layer-by-layer growth before the growth mode switches to vertical growth mode [29,35]. The film growth rates in these studies were around 3–4 nm/min. Regula et al. measured the sheet resistances of films ranging from 20 nm to 1400 nm and found that the sheet resistance was almost independent of the thickness. It was concluded that the current was flowing mainly in an interfacial layer of about 20 nm in thickness corresponding to the region of the film that demonstrated a (001)-texture.

To study the switching from layer-by-layer growth mode to vertical growth mode, films with three different thicknesses were deposited: 20 nm, 35 nm, 110 nm. Substrate temperature was kept at 700 °C and the pressure was 6.67 Pa using pure $H_2S$ (20 sccm) as processing gas. XRD-diffractograms from these films are shown in Fig. 5 and it is seen that (100)/(101) peaks clearly appear for the thickest film which indicates that at least parts of the film have switched over to vertical growth mode. Fig. 6a and b show TEM images for the thickest film. It is clearly seen that the (001)-texture can be maintained throughout the whole film which is 110 nm thick. This would indicate a thicker (001)-texture than found in previous studies [29,35]. The film structure is however not the same all over the film. This is of course indicated already from the (100)/(101) peaks in the XRD (with a probing size of several tens of $mm^2$). At other spots on the sample it is possible to observe a switch to the perpendicular growth mode. One example of this may be found in Fig. 7a and b which show how a crystal defect [29] serves as a seed location for vertical growth at a film thickness less than 20 nm. Fig. 7b demonstrates how the growth at the edges, perpendicular to the c-axis of the crystal, is much faster (about a factor of 5) than the growth along the c-axis, i.e. in the (001) direction. This demonstrates that once the film growth has switched over to vertical growth mode, it is not possible to obtain a high quality (001)-textured film regardless of post annealing/sulfurization procedure. It is therefore paramount to maintain the (001)-texture throughout the film to have a chance of improving the film quality in terms of larger grain size and higher sulfur content by an additional annealing step in $H_2S$ atmosphere. In order to estimate how large portion of the film that exhibits layer-by-layer growth (on the macroscopic scale), we conducted four point probe measurements on the thickest film (110 nm) and the thinnest film (20 nm). These measurements showed sheet resistances of around 6 MΩ/sq and 15 MΩ/sq for the thickest and thinnest film respectively, corresponding to 30 Ωcm and 66 Ωcm. This is of the same order of magnitude that has been obtained by others [31,35,49]. Since the thickest film exhibits a resistivity about twice as high as the 5–6 times thinner film, it can be concluded that a significant portion of the film has a layer-by-layer structure throughout the film depth. This is in contrast to what was observed by Regula et al. who reported a sheet resistance that was only increased by a factor of 1.5 when the films thickness increased from 20 nm to 1400 nm [35].

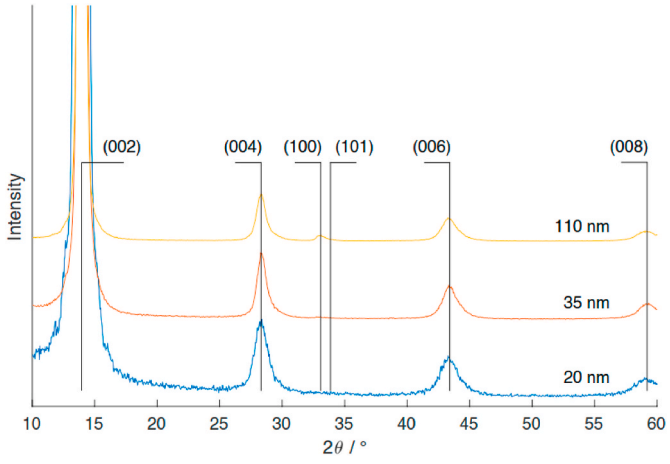


**Fig. 5.** XRD for films with different thicknesses deposited at 6.67 Pa, 700 °C, and pure $H_2S$. Error bars are within the size of the markers.

We believe that part of the explanation to be able to grow such thick (001)-textured films is the extremely low growth rate of about 0.3 nm/min (obtained at 6.67 Pa in this study) which is one order of magnitude slower than that of Regula et al. and Ellmer et al. who both demonstrated only tens of nm thick (001)-textured films [29,35]. The low growth rate is a consequence of the high processing pressure and the large target-to-substrate distance [50]. The high pressure and large distance is also advantageous since it will effectively thermalize energetic particles originating from the target [45]. Therefore, the low growth rate is accompanied by a significantly lower kinetic particle energy at the substrate, which alters the growth conditions and influences the texture of the coating.

The results so far have concerned $SiO_2$/Si substrates. In Fig. 8 we present results of depositions on sapphire and unoxidized Si substrates together with the $SiO_2$/Si presented above. The diffractograms are normalized to the (002) reflection peak height. The Laue oscillations around the (002) peak indicate a smooth and uniform film. Besides additional peaks from the substrate in the sapphire case, the diffractogram envelopes are similar. The FWHM of the $WS_2$ reflections are also similar. This can be explained by a weak interaction between the deposited $WS_2$ and the substrate.

Since sapphire has a hexagonal symmetry, similar to $WS_2$, this might have helped to align the nucleated grains and enable epitaxial growth of $WS_2$ on such substrates [7]. However, no significant difference in quality between the films grown was observed.

## 4. Conclusions

We have sputter deposited $WS_2$ thin films by reactive sputtering from a $WS_2$ target in an Ar/$H_2S$ atmosphere. This is an industrially compatible and scalable process, capable of producing wafer scale $WS_2$ films on $SiO_2$/Si, Si, and sapphire. Films were deposited at different processing

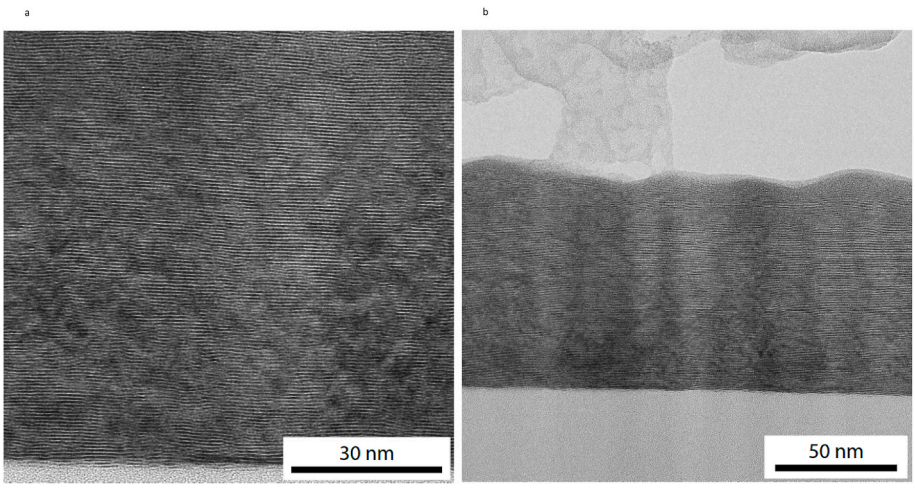


**Fig. 6.** TEM images of a 110 nm thick film deposited at 700 °C, 6.67 Pa, pure $H_2S$ (a) close-up view of the (001)-textured growth revealing a relatively low density of bifurcations and lattice defects (b) zoomed out view showing how the (001) growth extends throughout the whole film.

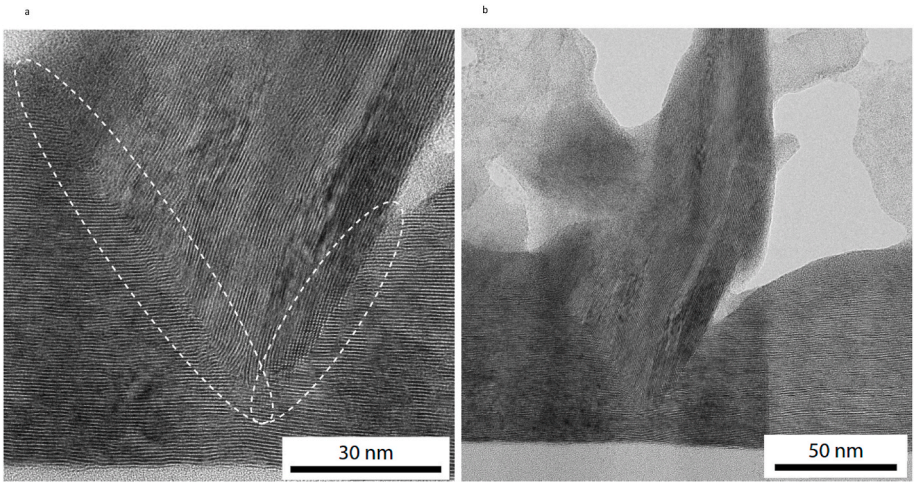


**Fig. 7.** TEM images of a 110 nm thick film deposited at 700 °C, 6.67 Pa, and pure $H_2S$ (a) close-up view of the (001)-textured growth switching over to (100)/(101) growth due to lattice defects/sulfur vacancies. The borders between the (001) and (100)/(101) textures are circled. (b) Zoomed out view illustrating how the (100)/(101) growth is much faster (about 5 times) than the (001) growth as a consequence of the much higher surface energy at the edge of the (001)-plane.

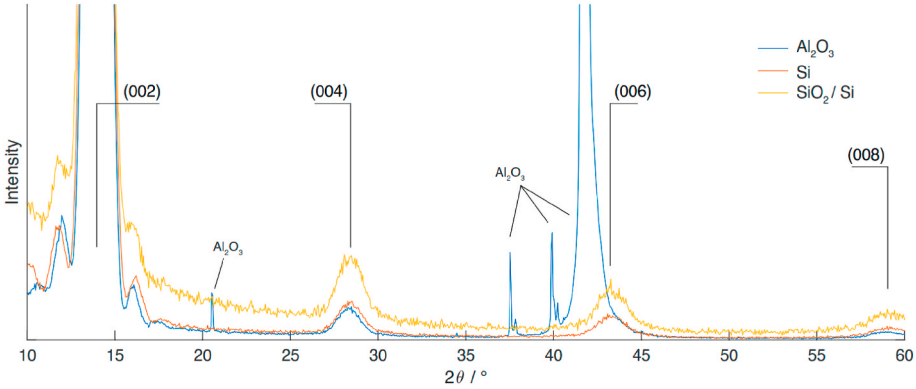


**Fig. 8.** XRD for 5 nm thick films deposited at 700 °C, 6.67 Pa, and pure $H_2S$ onto different substrates. The diffractogram intensity is normalized to the main (002) reflection. Apart from a background the FWHM of the (002) reflection is the same for the three different depositions. In the sapphire case the additional peaks originate from the substrate.

pressures (0.67 Pa–6.67 Pa), substrate temperatures (up to 700 °C) and relative amounts of $H_2S$ (0%–100%) in the Ar/$H_2S$ gas mixture. High processing pressure and high substrate temperature were beneficial for obtaining a good film quality in terms of crystallinity and stoichiometry. At the highest pressure and temperature, we investigated the influence of different amounts of $H_2S$ in the gas mixture. We were not able to

obtain fully stoichiometric films and the highest [S]/[W] ratio was 1.94. The addition of the $H_2S$ resulted in a slightly better film quality while it did not improve the [S]/[W] ratio. For 60–100% of $H_2S$ in the gas, there were significant amounts (5–10%) of hydrogen in the films. Further, the [S]/[W] ratio was reduced for $H_2S$ contents over 60%.

Owing to its low surface energy, the $WS_2$ films always start to grow in a layer-by-layer fashion, i.e. (001)-texture, while after tens of nm, the growth may easily be switched into a growth mode where the layers are perpendicular to the substrate, i.e. (100)/(101)-texture. The switch in growth mode is caused by lattice defects e.g. sulfur vacancies or bifurcations [29]. Once the switch to (100)/(101)-texture occurs, it is not possible to obtain the (001)-texture again. Nonetheless, we were able to deposit a 110 nm films that exhibit only (001)-textured growth throughout the film thickness. However, at several positions also this film showed switching over to (100)/(101)-texture.

We believe that key components that promote high quality film growth are very low deposition rate and large target-to-substrate distance. Furthermore 40–60% $H_2S$ in the gas mixture gives optimized films in terms of the combination of crystallinity, [S]/[W] ratio, and reduced hydrogen impurities. Films grown within this range of $H_2S$ in the gas might have a higher chance of maintaining the (001)-texture for thicker films. Such films may be further improved in a post annealing step in pure $H_2S$.

## Declaration of competing interest

The authors declare that they have no known competing financial interests or personal relationships that could have appeared to influence the work reported in this paper.

## Acknowledgements

This work was supported by the FLAG-ERA grant LaMeS, by the Swedish Research Council VR Grant 2017–06816; by the French National Research Agency grant ANR-17-GRF1-0001-03 and by the Carl Tryggers Foundation contract CTS 19:258. A.L. acknowledges the support from the Swedish Research Council (Grants No. 2014–6463 and No. 2018–05336) and Marie Sklodowska Curie Actions (Cofund, Project INCA 600398). A.F. acknowledges funding by FLAG-ERA Graphene Basic Research 2 2017 in project LaMeS DFG project number 400335214. Financial support of the tandem accelerator infrastructure by VR-RFI (contract #2017-00646_9) as well as the Swedish Foundation for Strategic Research (SSF) under contract RIF14-005 is gratefully acknowledged. Lars Riekehr is acknowledged for the TEM analysis.

## References

[1] K.S. Novoselov, A.K. Geim, S.V. Morozov, D. Jiang, Y. Zhang, S.V. Dubonos, I. V. Grigorieva, A.A. Firsov, Electric field effect in atomically thin carbon films, Science 306 (5696) (2004) 666–669.
[2] A. Zavabeti, A. Jannat, L. Zhong, A.A. Haidry, Z.J. Yao, J.Z. Ou, Two-dimensional materials in large-areas: synthesis, properties and applications, Nano-Micro Lett. 12 (1) (2020).
[3] C. Muratore, A.A. Voevodin, N.R. Glavin, Physical vapor deposition of 2D Van der Waals materials: a review, Thin Solid Films 688 (2019).
[4] X. Tong, K.L. Liu, M.Q. Zeng, L. Fu, Vapor-phase growth of high-quality wafer-scale two-dimensional materials, Infomatics 1 (4) (2019) 460–478.
[5] N. Mounet, M. Gibertini, P. Schwaller, D. Campi, A. Merkys, A. Marrazzo, T. Sohier, I.E. Castelli, A. Cepellotti, G. Pizzi, N. Marzari, Two-dimensional materials from high-throughput computational exfoliation of experimentally known compounds, Nat. Nanotechnol. 13 (3) (2018) 246–+.
[6] M. Ezawa, E. Salomon, P. De Padova, D. Solonenko, P. Vogt, M. Dávila, A. Molle, T. Angot, G. Le Lay, Fundamentals and functionalities of silicene, germanene, and stanene, La Rivista del Nuovo Cimento 41 (2018) 175–224.
[7] C.Y. Lan, C. Li, J.C. Ho, Y. Liu, 2D WS2: from vapor phase synthesis to device applications, Adv. Electron. Mater..
[8] M. Samadi, N. Sarikhani, M. Zirak, H. Zhang, H.L. Zhang, A.Z. Moshfegh, Group 6 transition metal dichalcogenide nanomaterials: synthesis, applications and future perspectives, Nanoscale Horizons 3 (2) (2018) 90–204.
[9] M. Bernardi, M. Palummo, J.C. Grossman, Extraordinary sunlight absorption and one nanometer thick photovoltaics using two-dimensional monolayer materials, Nano Lett. 13 (8) (2013) 3664–3670.
[10] Y.L. Li, A. Chernikov, X. Zhang, A. Rigosi, H.M. Hill, A.M. van der Zande, D. A. Chenet, E.M. Shih, J. Hone, T.F. Heinz, Measurement of the optical dielectric function of monolayer transition-metal dichalcogenides: MoS2, MoSe2, WS2, and WSe2, Phys. Rev. B 90 (20) (2014).
[11] Y. Fan, Y.Q. Zhou, X.C. Wang, H.J. Tan, Y.M. Rong, J.H. Warner, Photoinduced Schottky barrier lowering in 2D monolayer WS2 photodetectors, Adv. Optic. Mater. 4 (10) (2016) 1573–1581.
[12] V. Shautsova, S. Sinha, L.L. Hou, Q.Y. Zhang, M. Tweedie, Y. Lu, Y.W. Sheng, B. F. Porter, H. Bhaskaran, J.H. Warner, Direct laser patterning and phase transformation of 2D PdSe2 films for on demand device fabrication, ACS Nano 13 (12) (2019) 14162–14171.
[13] X.B. Yan, Q.O.L. Zhao, A.P. Chen, J.H. Zhao, Z.Y. Zhou, J.J. Wang, H. Wang, L. Zhang, X.Y. Li, Z.A. Xiao, K.Y. Wang, C.Y. Qin, G. Wang, Y.F. Pei, H. Li, D.L. Ren, J.S. Chen, Q. Liu, Vacancy-induced synaptic behavior in 2D WS2 nanosheet-based memristor for low-power neuromorphic computing, Small 15 (24) (2019).
[14] Z.H. Jin, X.D. Li, J.T. Mullen, K.W. Kim, Intrinsic transport properties of electrons and holes in monolayer transition-metal dichalcogenides, Phys. Rev. B 90 (4) (2014).
[15] W.X. Zhang, Z.S. Huang, W.L. Zhang, Y.R. Li, Two-dimensional semiconductors with possible high room temperature mobility, Nano Res. 7 (12) (2014) 1731–1737.
[16] W.S. Hwang, M. Remskar, R.S. Yan, V. Protasenko, K. Tahy, S.D. Chae, P. Zhao, A. Konar, H.L. Xing, A. Seabaugh, D. Jena, Transistors with chemically synthesized layered semiconductor WS2 exhibiting 10(5) room temperature modulation and ambipolar behavior, Appl. Phys. Lett. 101 (1) (2012).
[17] D. Ovchinnikov, A. Allain, Y.S. Huang, D. Dumcenco, A. Kis, Electrical transport properties of single-layer WS2, ACS Nano 8 (8) (2014) 8174–8181.
[18] Y. Cui, R. Xin, Z.H. Yu, Y.M. Pan, Z.Y. Ong, X.X. Wei, J.Z. Wang, H.Y. Nan, Z.H. Ni, Y. Wu, T.S. Chen, Y. Shi, B.G. Wang, G. Zhang, Y.W. Zhang, X.R. Wang, High-performance monolayer WS2 field-effect transistors on high-kappa dielectrics, Adv. Mater. 27 (35) (2015) 5230–5234.
[19] J.F. Jiang, Q.H. Zhang, A.Z. Wang, Y. Zhang, F.Q. Meng, C.C. Zhang, X.J. Feng, Y. P. Feng, L. Gu, H. Liu, L. Han, A facile and effective method for patching sulfur vacancies of WS2 via nitrogen plasma treatment, Small 15 (36) (2019).
[20] Z. Mutlu, M. Ozkan, C.S. Ozkan, Large area synthesis, characterization, and anisotropic etching of two dimensional tungsten disulfide films, Mater. Chem. Phys. 176 (2016) 52–57.
[21] S. Hussain, M.F. Khan, M.A. Shehzad, D. Vikraman, M.Z. Iqbal, D.C. Choi, W. Song, K.S. An, Y. Seo, J. Eom, W.G. Lee, J. Jung, Layer-modulated, wafer scale and continuous ultra-thin WS2 films grown by RF sputtering via post-deposition annealing, J. Mater. Chem. C 4 (33) (2016) 7846–7852.
[22] Y. Jung, J. Shen, Y.H. Liu, J.M. Woods, Y. Sun, J.J. Cha, Metal seed layer thickness-induced transition from vertical to horizontal growth of MoS2 and WS2, Nano Lett. 14 (12) (2014) 6842–6849.
[23] C.M. Orofeo, S. Suzuki, Y. Sekine, H. Hibino, Scalable synthesis of layer-controlled WS2 and MoS2 sheets by sulfurization of thin metal films, Appl. Phys. Lett. 105 (8) (2014).
[24] K. Kang, S.E. Xie, L.J. Huang, Y.M. Han, P.Y. Huang, K.F. Mak, C.J. Kim, D. Muller, J. Park, High-mobility three-atom-thick semiconducting films with wafer-scale homogeneity, Nature 520 (7549) (2015) 656–660.
[25] A. Grundmann, C. McAleese, B. Conran, A. Pakes, D. Andrzejewski, T. Kummell, G. Bacher, K.B.K. Teo, M. Heuken, H. Kalisch, A. Vescan, MOVPE of Large-Scale MoS2/WS2, WS2/MoS2, WS2/Graphene and MoS2/Graphene 2D-2D heterostructures for optoelectronic applications, MRS Adv. 5 (31–32) (2020) 1625–1633.
[26] T.H. Choudhury, H. Simchi, R. Boichot, M. Chubarov, S.E. Mohney, J.M. Redwing, Chalcogen precursor effect on cold-wall gas-source chemical vapor deposition growth of WS2, Cryst. Growth Des. 18 (8) (2018) 4357–4364.
[27] J. Park, W. Lee, T. Choi, S.H. Hwang, J.M. Myoung, J.H. Jung, S.H. Kim, H. Kim, Layer-modulated synthesis of uniform tungsten disulfide nanosheet using gas-phase precursors, Nanoscale 7 (4) (2015) 1308–1313.
[28] K. Ellmer, Preparation routes based on magnetron sputtering for tungsten disulfide (WS2) films for thin-film solar cells, Phys. Status Solidi B-Basic Solid State Phys. 245 (9) (2008) 1745–1760.
[29] V. Weiss, S. Seeger, K. Ellmer, R. Mientus, Reactive magnetron sputtering of tungsten disulfide (WS2-x) films: influence of deposition parameters on texture, microstructure, and stoichiometry, J. Appl. Phys. 101 (10) (2007).
[30] K. Ellmer, S. Seeger, I. Sieber, W. Bohne, J. Rohrich, E. Strub, R. Mientus, Reactive magnetron sputtering of highly (001)-textured WS2-x films: influence of Ne+, Ar+ and Xe+ ion bombardment on the film growth, Phys. Status Solidi A-Appl. Mat. 203 (3) (2006) 497–503.
[31] S. Seeger, R. Mientus, J. Rohrich, E. Strub, W. Bohne, K. Ellmer, Electrical and optical properties of highly (001) textured WSx films deposited by reactive magnetron sputtering, Surf. Coating. Technol. 200 (1–4) (2005) 218–221.
[32] K. Ellmer, R. Mientus, S. Seeger, V. Weiss, Highly (001)-textured WS2-x films prepared by reactive radio frequency magnetron sputtering, Phys. Status Solidi A-Appl. Mat. 201 (14) (2004) R97–R100.
[33] K. Ellmer, C. Stock, K. Diesner, I. Sieber, Deposition of c(perpendicular to)-oriented tungsten disulfide (WS2) films by reactive DC magnetron sputtering from a W-target in Ar/H72S, J. Cryst. Growth 182 (3–4) (1997) 389–393.
[34] A. Ennaoui, S. Fiechter, K. Ellmer, R. Scheer, K. Diesner, Preparation of textured and photoactive 2H-WS2 thin films by sulfurization of WO3, Thin Solid Films 261 (1) (1995) 124–131.
[35] M. Regula, C. Ballif, J.H. Moser, F. Levy, Structural, chemical, and electrical characterisation of reactively sputtered WS/sub x/thin films, Thin Solid Films 280 (1–2) (1996) 67–75.

[36] C. Ballif, M. Regula, M. Remskar, R. Sanjines, F. Levy, Nanoscopic trigonal pyramidal crystallites in WS2-x sputtered thin films: a scanning tunnelling microscopy study of initial growth, Surf. Sci. 366 (2) (1996) L703–L708.
[37] M. Regula, C. Ballif, F. Levy, Growth and electrical properties of reactively sputtered WSx thin films, in: S. Pizzini, H.P. Strunk, J.H. Werner (Eds.), Polycrystalline Semiconductors Iv - Physics, Chemistry and Technology, Scitec Publications Ltd, Zug, 1996, pp. 335–340.
[38] E. Sarhammar, E. Strandberg, J. Sundberg, H. Nyberg, T. Kubart, S. Jacobson, U. Jansson, T. Nyberg, Mechanisms for compositional variations of coatings sputtered from a WS2 target, Surf. Coating. Technol. 252 (2014) 186–190.
[39] S. Tongay, J. Suh, C. Ataca, W. Fan, A. Luce, J.S. Kang, J. Liu, C. Ko, R. Raghunathanan, J. Zhou, F. Ogletree, J.B. Li, J.C. Grossman, J.Q. Wu, Defects activated photoluminescence in two-dimensional semiconductors: interplay between bound, charged, and free excitons, Sci. Rep. 3 (2013).
[40] K. Matsuura, T. Ohashi, I. Muneta, S. Ishihara, K. Kakushima, K. Tsutsui, A. Ogura, H. Wakabayashi, Low-carrier-density sputtered MoS2 film by vapor-phase sulfurization, J. Electron. Mater. 47 (7) (2018) 3497–3501.
[41] K. Komander, M. Moro, J. Saha, M. Wolff, D. Primetzhofer, Hydrogen induced lattice expansion and site occupation analyzed by ion beam methods, Nucl. Instrum. Methods Phys. Res. Sect. B Beam Interact. Mater. Atoms 486 (2021) 63–67.
[42] M. Mayer, SIMNRA, a simulation program for the analysis of NRA, RBS and ERDA, in: J.L. Duggan, I.L. Morgan (Eds.), Application of Accelerators in Research and Industry, Pts 1 and 2, Amer Inst Physics, Melville, 1999, pp. 541–544.
[43] A.J. Ying, C.E. Murray, I. Noyan, A rigorous comparison of X-ray diffraction thickness measurement techniques using silicon-on-insulator thin films, J. Appl. Crystallogr. 42 (3) (2009) 401–410.
[44] W.F. Yang, H. Kawai, M. Bosman, B.S. Tang, J.W. Chai, W.L. Tay, J. Yang, H. L. Seng, H.L. Zhu, H. Gong, H.F. Liu, K.E.J. Goh, S.J. Wang, D.Z. Chi, Interlayer interactions in 2D WS2/MoS2 heterostructures monolithically grown by in situ physical vapor deposition, Nanoscale 10 (48) (2018) 22927–22936.
[45] F.O.L. Johansson, P. Ahlberg, U. Jansson, S.L. Zhang, A. Lindblad, T. Nyberg, Minimizing sputter-induced damage during deposition of WS2 onto graphene, Appl. Phys. Lett. 110 (10) (2017).
[46] M. Genut, L. Margulis, G. Hodes, R. Tenne, Preparation and microstructure of WS2 thin films, Thin Solid Films 217 (1–2) (1992) 91–97.
[47] O. Lignier, G. Couturier, J. Tedd, D. Gonbeau, J. Salardenne, Photoactivity enhancement of WS2 sputtered thin films by use of nickel, Thin Solid Films 299 (1–2) (1997) 45–52.
[48] D.A. Rice, S.J. Hibble, M.J. Almond, K.A.H. Mohammad, S.P. Pearse, Novel low-temperature route to known (MnS and FeS2) and new (CrS3, MoS4 and WS5) transition-metal sulfides, J. Mater. Chem. 2 (8) (1992) 895–896.
[49] A. Jäger-Waldau, M.C. Lux-Steiner, G. Jäger-Waldau, E. Bucher, WS2 thin films prepared by sulphurization, Appl. Surf. Sci. 70–71 (1993) 731–736.
[50] E. Sarhammar, E. Strandberg, N. Martin, T. Nyberg, Sputter rate distribution and compositional variations in films sputtered from elemental and multi-element targets at different pressures, Int. J. Mater. Sci. Appl. 3 (2) (2014) 29.